Modeling of ideality factor value in n^+–p–p^+–Si structure

O.Ya. Olikh, O.V. Zavhorodnii

https://orcid.org/0000-0003-0633-5429 (Olikh)

Taras Shevchenko National University of Kyiv

64/13, Volodymyrska Street, City of Kyiv, Ukraine, 01601

e-mail: olikh@univ.kiev.ua

This paper presents the results of computer simulation of the ideality factor of silicon $n^+ - p - p^+$ structure with iron contamination. The Solar Cells Capacitance Simulator (SCAPS) was the tool used for numerical simulation of these devices. The iron concentration range of $10^{10} - 10^{13}$ cm^{-3}, acceptor doping level range of $10^{15} - 10^{17}$ cm^{-3}, temperature range of $290 - 340$ K, and base thickness range of $150 - 240$ μm were used in the investigation. The double diode model was used to extract the ideality factor. The following cases were considered: (i) uniformly distributed lone interstitial iron atoms; (ii) coexistence of non–uniformly distributed Fe$_i$ and Fe$_i$B$_s$ It has been shown that the ideality factor value determined by a hole occurring on the Fe$_i$ level, a trap location, and a intrinsic recombination contribution. The increase in base thickness leads to decrease in n value. The sign of change in ideality factor after Fe$_i$B$_s$ dissociation depends on temperature, doping level, and iron concentration.

Key words: ideality factor, silicon, n^+–p–p^+ structure, SCAPS, iron concentration

1   Introduction

In the literature, there are several models that describe the current–voltage $(I - V)$ characteristics of the solar cells (SCs). These models contain some parameters, which reflect the processes within the structures and are related to the main characteristics of the photovoltaic conversion. So single diode model with three parameters has been used to represent the SC static characteristic because of simplicity:

$$I = I_0 \left[\exp \left(-\frac{qV}{nkT} \right) - 1 \right] - I_{ph} \,, \tag{1}$$

were I_0 is the saturation current, n is the diode ideality factor, I_{ph} is the total current generated by solar cell. The ideality factor value indicates about a defect related recombination and directly determines open–circuit magnitude:

$$V_{oc} = \frac{nkT}{q} \ln \left(\frac{I_{ph}}{I_0} + 1 \right) \,. \tag{2}$$

Eq. (1) does not take into account a leakage current, a series losses of load current. Besides, the widely used double diode model is developed by considering the effect of recombination current loss in the depletion region [1–3]:

$$I = I_{01} \left[\exp \left(-\frac{q(V - R_s I)}{kT} \right) - 1 \right] + I_{02} \left[\exp \left(-\frac{q(V - R_s I)}{nkT} \right) - 1 \right] + \frac{V - R_s I}{R_{sh}} - I_{ph} \,, \tag{3}$$

where first term closely related to the recombination in the quasi–neutral region, second term describes the overall space charge region (SCR) recombination, R_s and $R_s h$ are the series and shunt resistance, respectively. In this case the relationship between the ideality factor and SC characteristics is more complicated. Певні приклади щодо взаємозв'язку n з напругою холостого ходу та fill factor рамках дво-діодної моделі можна знайти в [4]. Typically, the value of the ideality factor ranges from 1 to 2 for real devices and depends on ambient conditions and recombination center parameters, including the concentration of traps [5–9]. This makes the ideality factor an important parameter that can be used to describe the electrical behavior of photovoltaic devices and characterize the recombination in SCs [10].

One of the main obstacles of such a convenient and express method developing is the multiparameter relationship between the n value and the concentration of recombination centers. This paper attempts to get over these difficulties by the simulation of $I - V$ characteristic of silicon solar cells, the determination of ideality factor, and the study of n value depending on simulation parameters. In contrast to the previous paper [11] in this case the n^+–p–p^+-structure, which is closer to the real SC, is under consideration. Additionally the base thickness is known [12,13] to affect SC efficiency; therefore the paper considers the influence of this parameter on the ideality factor value.

The paper focuses on the case when the main recombination centers are the iron related defects. On the one hand, the iron atoms are one of the most common as well as the most harmful impurities in silicon solar cell. On the other hand, the $Fe_i B_s$ pairs can be readily dissociated by illumination [13]; the association reaction can take place when exposed in darkness for ten minutes [14]. Such a change in recombination center state should lead to a change in a ideality factor value, that is easy to obtain experimentally and to use to SC characterization. Therefore, the paper also pays attention to dependencies of n value change.

2   Simulation details

The calculation presented here uses $n^+ - p - p^+$ structure shown in inset in Fig. 1. Its main parts are the emitter layer with thickness d_n, the base with hole conductivity and thickness d_p and the p^+ layer with thickness d_{BSF} intended to back surface field (BSF) creation. BSF-layer is designed to increase the photovoltaic converter efficiency by reducing the losses concerned with surface recombination and such structure is widely used for both manufacturing of real solar cells and modeling [15–17].

The material of all layers was assumed to be monocrystalline silicon. The temperature dependencies of bandgap was calculated according to Pässler equations [18]. The bandgap narrowing, thermal carrier velocities, and free carrier effective mass were taken from Yan and Cuevas [19], Green [20], and O'Mara $et~al.$ [21], respectively. Data from Couderc $et~al.$ [22] were used to evaluate intrinsic carrier density and density of states effective masses. The temperature dependencies carrier mobilities were described by Klaassen's theory [23, 24].

It was assumed uniform doping with phosphorus (the emitter layer, concentration N_D) and boron (base and BSF–layer, concentrations N_A and N_{BSF}, respectively).

The following recombination processes were taken into account: i) the outside surface recombination with electron and hole velocities 10^3 cm/s; ii) the intrinsic recombination (radiative band–to–band and Auger with coefficients, which depend on temperature and doping level according to Nguyen *et al.* [25] and Altermatt *et al.* [26]); iii) the Shockley—Read-—Hall (SRH) recombination.

In the last case, as the base and BSF–layer uniform contaminant, iron is assumed to be in concentration N_{Fe}. It is well known that the iron atom locates in lone interstitial lattice position in silicon (Fe_i) or interacts with ionized acceptors and combines into Fe_iB_s pair. The two cases were under consideration. In the first one, uniformly distributed Fe_i with concentration N_{Fe} was assumed. Such case is realizing under constant illumination or immediately after its termination. The temperature independent donor level $E_{Fe_i} = E_V + 0.394$ eV [27–29] and electron $\sigma_{n,Fe} = 3.47 \times 10^{-15}T^{-1.48}$ m^2 and hole $\sigma_{p,Fe} = 4.54 \times 10^{-20} \exp\left(-\frac{0.05}{kT}\right)$ m^2 capture cross-sections [30, 31] are associated with Fe_i. In the second one, Fe_i and Fe_iB_s were coexistence. Their concentration were non–uniformly distributed through base and BSF–layer. The more details are presented elsewhere [11] and the representative examples of calculation are shown in Fig. 2. Such case is realizing under dark equilibrium condition. The Fe_iB_s is amphoteric defect and donor level $E_{FeB}^D = E_V + 0.10$ eV, $\sigma_{n,FeB}^D = 4 \times 10^{-17}$ m^2, $\sigma_{p,FeB}^D = 2 \times 10^{-18}$ m^2 and acceptor level $E_{FeB}^A = E_C - 0.26$ eV, $\sigma_{n,FeB}^A = 5.1 \times 10^{-13}T^{-2.5}$ m^2, $\sigma_{p,FeB}^A = 3.32 \times 10^{-14} \exp\left(-\frac{0.262}{kT}\right)$ m^2 [14, 27, 28, 30–32] are used in simulation.

The dark forward dark $I - V$ characteristic were generated by one-dimensional code SCAPS 3.3.08 [33, 34] over a voltage range up to 0.45 V with step 0.01 V. This software is widely applied in modeling various solar cells [15, 16, 35–39], silicon based devices including [15, 16, 39]. The used parameters are listed in Table 1. Thus, the varied parameters were the boron concentrations in the base, iron concentration, base thickness and temperature. Taking into account two defect configuration, 15048 structures were simulated. The examples of $I - V$ curve are shown in Fig. 1.

The simulated $I - V$ characteristic were fitted by following equation:

$$I = I_{01}\left[\exp\left(-\frac{qV}{kT}\right) - 1\right] + I_{02}\left[\exp\left(-\frac{qV}{nkT}\right) - 1\right]. \tag{4}$$

Eq. (4) corresponds to the dark double diode model with neglected both series and shunt resistances. The first diode represents the "ideal" diode, describing the so–called diffusion current characterized by a saturation current I_{01}, and the second diode is the so–called recombination current, characterized by the saturation current I_{02} and ideality factor n [3]. n, I_{01}, and I_{02} were taken as fitting parameters and the meta–heuristic method IJAVA [40] was used. The representative results of the fitting are shown in Fig. 1 as well.

In the case of lone unpaired Fe_i the following value were calculated: n_{Fe}^{srh} is the ideality factor if the SRH recombination was taken into account only; n_{Fe} is the ideality factor if the both SRH recombination and intrinsic recombination were allowed; $\delta n_{Fe}^{srh} = n_{Fe}^{srh} - n_{Fe}$ characterizes the influence of intrinsic recombination on ideality factor value. In the case of Fe_iB_s and Fe_i coexistence the n_{FeB}^{srh}, n_{FeB}, $\delta n_{FeB}^{srh} = n_{FeB}^{srh} - n_{FeB}$ were calculated (indices had the same meaning). Besides, the change of the ideality factor after Fe_iB_s association $\delta n_{Fe-FeB} = n_{Fe} - n_{FeB}$ was calculated as well.

3 Results and discussion

Figs. 3–5 show the typical simulated dependencies of ideality factor value on temperature and both iron and boron concentration. Note that the $\delta n_{\mathrm{Fe}}^{\mathrm{srh}}$ surfaces (number 5, orange) do not shown if they practically coincide with the $\delta n_{\mathrm{FeB}}^{\mathrm{srh}}$ surfaces (4, yellow).

It should paid attention to Fig. 2 before a discussion of obtained dependencies. Firstly, the presented data testify to the primary role of unpaired interstitial iron in recombination even in the case of $\mathrm{Fe}_i\mathrm{B}_s$ and Fe_i coexistence. In fact, donor $E_{\mathrm{FeB}}^{\mathrm{D}}$ level is below Fermi level and therefore its probability of capture of non–equilibrium electron is small. Additionally, the ideality factor value above all associated with a SCR recombination and the Fe_i concentration exceeds the $\mathrm{Fe}_i\mathrm{B}_s$ concentration in $2/3$ thickness of space charge region. And it is confirmed by the similarity of dependencies of n_{FeB} (surfaces 1, red) and n_{Fe} (surfaces 2, cyan) on Figs. 3–5. Secondly, the unpaired iron atom concentration can be big enough in the case of $\mathrm{Fe}_i\mathrm{B}_s$ and Fe_i coexistence as well and it increases with temperature rise and decrease in doping level. For example, the Fe_i concentration in the quasi–neutral region of base reaches 23 (or 3) percent of N_{Fe} at $T = 340$ K and $N_{\mathrm{A}} = 10^{15}$ cm^{-3} (or 10^{16} cm^{-3}). That is, under these conditions, the concentration of unpaired iron atoms in the dark and $N_{\mathrm{Fe}} = 10^{13}$ cm^{-3} is larger than ones under illumination and $N_{\mathrm{Fe}} = 10^{11}$ cm^{-3}. Finally, as only ionized iron Fe_i^+ (unlike to neutral iron Fe_i^0) actively takes part in the SRH recombination, then these processes efficiently occur at $x \geq 0.6 W_p$ (where W_p is the SCR depth). And the area of processes, which determines ideality factor value, shifts away from the $p - n$ junction with increase in doping level.

Several determinants must be taken into account when analyzing the dependencies of the ideality factor on the temperature and boron concentration of boron. Namely.

i) The occurring of hole on the Fe_i level, which determines the recombination efficiency. Accordingly to the Fermi–Dirac statistics, the probability of hole occupation in a non–degenerate $p-$type semiconductor with full acceptor depletion can be expressed as

$$f_p = \frac{1}{1 + \frac{N_V(T)}{N_{\mathrm{A}}} \exp\left(\frac{E_V - E_{\mathrm{Fe}_i}}{kT}\right)} .\tag{5}$$

It has been shown earlier [4] the $f_p(T, N_{\mathrm{A}})$ dependence is generally similar to observed dependence of ideality factor dependence. In particular, if f_p is close to one (high N_{A} value and low temperature), this dependence changes slowly, n does not depend on temperature and slowly rises with increase in doping level — see Figs.4(b),(c); 5(a). If N_{A} decreases or (and) T increases, the level is filled by electron in a sufficiently narrow range of arguments, the SRH recombination ceases, and the ideality factor value sharply reduces — Figs.3, 4(a); 5(b).

ii) The balance of the defect related recombination and the intrinsic recombination. SRH recombination generally causes increase in ideality factor value; if the defect related recombination is dominant, the value often reported in publications is $n = 2$. The radiative band–to–band and Auger recombinations are enhanced by the increase in both free charge carrier concentration (doping level) and temperature [25,26]). In this case, the ideality factor reduces and the values $\delta n_{\mathrm{Fe}}^{\mathrm{srh}}$ and $\delta n_{\mathrm{FeB}}^{\mathrm{srh}}$

become nonzero. This effect is observed in the corners of surfaces on Figs. 3(a); 4(b),(c); 5.

The change in the impurity iron concentration has almost no effect on the nature of the n dependence on other parameters. However, the N_{Fe} rise is expectedly accompanied by an increase in the ideality factor value (see Figs. 4, 5), which is almost linear with respect to $\ln(N_{Fe})$. An exception is observed only when the level Fe_i is filled by an electron ($n < 1.06$). At the same time, the intrinsic recombination has a greater contribution at low iron concentration and same other parameters; and the sharp decrease in the ideality factor value is observed in the wake of the low impurity concentration. The striking examples are shown on Figs. 4(b),(c).

Taking into account Eq. (3), one can see that the the ideality factor appears in the item, connected to the SCR recombination. Therefore seemingly, n should not depend on the thickness of the n^+–p–p^+ structure base. However, such a dependence is observed (see Fig. 6(a)) and the ideality factor decreases with increase in thickness. This is evidence that the n value is influenced by processes in the quasi-neutral region as well. The ideality factor changes in similar way in both lone unpaired Fe_i and Fe_iB_s and Fe_i coexistence cases and described well by a linear dependence

$$n = n_0 - \beta\, d_p. \tag{6}$$

where β is the ideality factor thickness coefficient. The maximum effect of thickness is observed at middle $1.05 < n < 1.25$ value. Figs. 6(b)–(d) show the dependencies of β on the other simulation parameters. One can see that the d_p influence on n generally intensifies with the increasing of temperature as well as decreasing of concentrations of both boron and iron. Decrease in relative contribution of SRH recombination due to electron filling of Fe_i level as well as due to the intensification of intrinsic recombination causes a decrease in the β module. In addition, Fig. 7 shows the dependencies of the electron diffusion length (L_n) in the base on the concentration lone unpaired Fe_i, calculated by using SCAPS. Apparently the influence of base thickness is observed in the $L_n > d_p$ case only, and this is the reason that $\beta \approx 0$ at $n > 1.3$.

Also Figs. 3–5 show dependencies of the ideality factor change after pairing of interstitial iron δn_{Fe-FeB} — see surfaces 3, blue. Since the association reaction leads to the depression of SRH recombination, it was expected that $n_{FeB} < n_{Fe}$ and $\delta n_{Fe-FeB} > 0$ at all parameters values. The examples of such anticipated dependencies are shown on Figs. 4(b),(c) and 5(a). In this case δn_{Fe-FeB} increases with increasing in boron concentration and does not practically depend on temperature and iron concentration. Exceptions are only observed if the contribution of intrinsic recombination increases and the δn_{Fe-FeB} decreases: see Fig. 4(b),(c) at high temperature and low iron concentration or Fig. 5(a) at high doping level and slight concentration of trap.

However, it was turned out that case of $n_{FeB} > n_{Fe}$ has been realized as well — see Figs. 3, 4(a), 5(b). The regions of negative δn_{Fe-FeB} value are observed in the vicinity of ideality factor decrease, which is induced by occupation of Fe_i level. The reason of $n_{FeB} > n_{Fe}$ could be the difference in the Fermi level location in the cases of lone unpaired Fe_i and Fe_iB_s and Fe_i coexistence. However, calculations have shown that such difference does not exceed 5×10^{-6} eV and cannot be the cause of the detected effect.

Fig. 8 presents the spatial distributions of recombinantly active interstitial iron atoms before and after the pairs formation and transition to the dark equilibrium state. It is evidently that the degree of decrease in the Fe_i^+ concentration depends on the distance to the $p - n$–junction. In our opinion, the namely change in the $N_{Fe_i^+}$ profile is the reason of the rise of ideality factor resistance to temperature and doping level in the case of Fe_iB_s and Fe_i coexistence. At that the effect depends on the total iron concentration: the increase in N_{Fe} value leads to the n decay at higher temperature (Fig. 4(a)) as well as at lower boron concentration (Fig. 5(b)).

In turn, the δn_{Fe-FeB} value depends as well on the iron concentration at neighborhood of $n_{FeB} > n_{Fe}$. As a result, δn_{Fe-FeB}, along with n_{Fe} and n_{FeB}, can be used to estimate the impurity concentration by parameters of $I - V$ characteristic.

4   Conclusion

The diode ideality factor of silicon $n^+ - p - p^+$ structure with iron contamination has been studied via computer simulation. The data used in the simulations were the following. The iron concentration ranged from 10^{10} to 10^{13} cm^{-3}, the acceptor doping level — from 10^{15} to 10^{17} cm^{-3}, the temperature — from 290 to 340 K, and the base thickness — from 150 to 240 μm. It has been shown that the temperature and doping level dependencies of the ideality factor value are mainly determined by a hole occurring on the Fe_i level. The n dependence on iron concentration is a monotonic function. Additionally, not only defect concentration but also its location influences on ideality factor value. The intrinsic recombination causes the decrease in the ideality factor value at a high temperature and doping level as well as at a low iron concentration. It has also been found that the base thickness influences on ideality factor if it exceeds the minority carrier diffusion length. The increase in base thickness leads to decrease in n value. The investigation has revealed that the ideality factor in Fe_iB_s and Fe_i coexistence case can exceed ones in lone unpaired Fe_i case. The ideality factor change after Fe_iB_s dissociation can be used to contaminant concentration evaluation.

5   Acknowledgements

References

[1] K. Ishaque, Z. Salam, H. Taheri, Sol. Energy Mater. Sol. Cells **95**, 586 (2011); https://doi.org/10.1016/j.solmat.2010.09.023

[2] A. J. Bühler, A. Krenzinger, Progress in Photovoltaics: Research and Applications **21**, 884 (2013); https://doi.org/10.1002/pip.2170

[3] O. Breitenstein, Opto–Electronics Review **21**, 259 (2013); https://doi.org/10.2478/s11772-013-0095-5

[4] O. Olikh, Superlattices Microstruct. **117**, 173 (2018); https://doi.org/10.1016/j.spmi.2018.03.027

[5] J. Beier, B. Voss, Conference Record of the Twenty Third IEEE Photovoltaic Specialists Conference, 321 (1993); https://doi.org/10.1109/PVSC.1993.347163

[6] K. McIntosh, P. Altermatt, G. Heiser, 16th European Photovoltaic Solar Energy Conference: Proceedings of the International Conference and Exhibition, 250 (2000)

[7] A. Kaminski *et al.*, Conference Record of the Twenty Fifth IEEE Photovoltaic Specialists Conference, 573 (1996); https://doi.org/10.1109/PVSC.1996.564071

[8] Z. Hameiri, K. McIntosh, G. Xu, Sol. Energy Mater. Sol. Cells **117**, 251 (2013); https://doi.org/10.1016/j.solmat.2013.05.040

[9] A. S. H. van der Heide, A. Schonecker, J. H. Bultman, W. C. Sinke, Progress in Photovoltaics: Research and Applications **13**, 3 (2005); https://doi.org/10.1002/pip.556

[10] L. Duan *et al.*, IEEE Journal of Photovoltaics **8**, 1701 (2018); https://doi.org/10.1109/JPHOTOV.2018.2870722

[11] O. Olikh, Superlattices Microstruct. **136**, 106309 (2019); https://doi.org/10.1016/j.spmi.2019.106309

[12] A. V. Sachenko *et al.*, Tech. Phys. Lett. **44**, 873 (2018); https://doi.org/10.1134/S1063785018100139

[13] J. Schmidt, Progress in Photovoltaics: Research and Applications **13**, 325 (2005); https://doi.org/10.1002/pip.594

[14] W. Wijaranakula, J. Electrochem. Soc. **140**, 275 (1993); https://doi.org/10.1149/1.2056102

[15] E. Hu *et al.*, Renewable Energy **77**, 442 (2015); https://doi.org/10.1016/j.renene.2014.12.049

[16] A. Hamache, N. Sengouga, A. Meftah, M. Henini, Radiat. Phys. Chem. **123**, 103 (2016); https://doi.org/10.1016/j.radphyschem.2016.02.025

[17] G. Azzouzi, W. Tazibt, Energy Procedia **41**, 40 (2013); https://doi.org/10.1016/j.egypro.2013.09.005

[18] R. Pässler, Phys. Rev. B **66**, 085201 (2002); https://doi.org/10.1103/PhysRevB.66.085201

[19] D. Yan, A. Cuevas, J. Appl. Phys. **116**, 194505 (2014); https://doi.org/10.1063/1.4902066

[20] M. A. Green, J. Appl. Phys. **67**, 2944 (1990); https://doi.org/10.1063/1.345414

[21] W. O'Mara, R. Herring, L. Hant, *Handbook of semiconductor silicon technology* (Noyes Publications, New Jersey, 1990)

[22] R. Couderc, M. Amara, M. Lemiti, J. Appl. Phys. **115**, 093705 (2014); https://doi.org/10.1063/1.4867776

[23] D. Klaassen, Solid-State Electron. **35**, 953 (1992); https://doi.org/10.1016/0038-1101(92)90325-7

[24] R. Hull, *Properties of crystalline silicon* (Institution of Engineering and Technology, London, 1999)

[25] H. T. Nguyen, S. C. Baker-Finch, D. Macdonald, Appl. Phys. Lett. **104**, 112105 (2014); https://doi.org/10.1063/1.4869295

[26] P. P. Altermatt, J. Schmidt, G. Heiser, A. G. Aberle, J. Appl. Phys. **82**, 4938 (1997); https://doi.org/10.1063/1.366360

[27] S. Rein, S. W. Glunz, J. Appl. Phys. **98**, 113711 (2005); https://doi.org/10.1063/1.2106017

[28] J. D. Murphy, K. Bothe, M. Olmo, V. V. Voronkov, R. J. Falster, J. Appl. Phys. **110**, 053713 (2011); https://doi.org/10.1063/1.3632067

[29] H. Kohno, H. Hieslmair, A. A. Istratov, E. R. Weber, Appl. Phys. Lett. **76**, 2734 (2000); https://doi.org/10.1063/1.126459

[30] F. E. Rougieux, C. Sun, D. Macdonald, Solar Energy Materials and Solar Cells **187**, 263 (2018); https://doi.org/10.1016/j.solmat.2018.07.029

[31] B. B. Paudyal, K. R. McIntosh, D. H. Macdonald, 34th IEEE Photovoltaic Specialists Conference (PVSC), 1588 (2009)

[32] A. A. Istratov, H. Hieslmair, E. Weber, Applied Physics A: Materials Science & Processing **69**, 13 (1999); https://doi.org/10.1007/s003390050968

[33] M. Burgelman, P. Nollet, S. Degrave, Thin Solid Films **361**–**362**, 527 (2000); https://doi.org/10.1016/S0040-6090(99)00825-1

[34] K. Decock, S. Khelifi, M. Burgelman, Thin Solid Films **519**, 7481 (2011); https://doi.org/10.1016/j.tsf.2010.12.039

[35] M. Cappelletti, G. Casas, A. Cédola, E. P. y Blancá, B. M. Soucase, Superlattices Microstruct. **123**, 338 (2018); https://doi.org/10.1016/j.spmi.2018.09.023

[36] M. Mostefaoui, H. Mazari, S. Khelifi, A. Bouraiou, R. Dabou, Energy Procedia **74**, 736 (2015); https://doi.org/10.1016/j.egypro.2015.07.809

[37] C.-H. Huang, W.-J. Chuang, Vacuum **118**, 32 (2015); https://doi.org/10.1016/j.vacuum.2015.03.008

[38] F. Azri, A. Meftah, N. Sengouga, A. Meftah, Solar Energy **181**, 372 (2019); https://doi.org/10.1016/j.solener.2019.02.017

[39] B. Zhao, J. Zhou, Y. Chen, Physica B: Condensed Matter **405**, 3834 (2010); https://doi.org/10.1016/j.physb.2010.06.012

[40] K. Yu, J. Liang, B. Qu, X. Chen, H. Wang, Energy Conversion and Management **150**, 742 (2017); https://doi.org/10.1016/j.enconman.2017.08.063

Table 1. Parameters' values used in the simulation

Fig. 1. Simulated I–V characteristic (marks) and its fitting by Eq. (4) (solid lines 1 and 4). The dashed (3, 6) and dotted–dashed (2, 5) lines represent the diffusion and recombination currents respectively. $N_A = 10^{17}$ cm^{-3}, $N_{Fe} = 10^{13}$ cm^{-3}, $T = 340$ K, $d_p = 180$ μm. The results for lone unpaired Fe$_i$ (circles, curves 4–6, red) as well as for Fe$_i$B$_s$ and Fe$_i$ coexistence (squares, curves 1–3, black) are presented.

Inset: Structure, which are used in simulation.

Fig. 2. The calculated base and SBF–layer distribution of Fermi level position (a, solid lines), unpaired interstitial iron concentration (b, dotted lines), and Fe$_i$B$_s$ pair concentration (b, solid lines) at $V = 0$. N_A, cm^{-3}: 10^{15} (curves 1, 2), 10^{16} (3, 4), 10^{17} (5, 6); T, K: 290 (1, 3, 5), 340 (2, 4, 6); $N_{Fe} = 10^{13}$ cm^{-3}; $d_p = 180$ μm. The positions of Fe$_i$ donor level (dotted–dashed line) and Fe$_i$B$_s$ donor level (dashed line) are shown in the panel (a) as well.

Fig. 3. Ideality factor and its change as a function of the temperature and acceptor (boron) concentration. N_{Fe}, cm^{-3}: 10^{10} (a), 10^{13} (b); $d_p = 240$ μm. Surface 1 (red) reflects the n_{FeB} dependance, 2 (cyan) $- n_{Fe}$, 3 (blue) $- \delta n_{Fe-FeB}$, 4 (yellow) $- \delta n_{FeB}^{srh}$, 5 (orange) $- \delta n_{Fe}^{srh}$.

Fig. 4. Ideality factor and its change as a function of the temperature and iron concentration. N_A, cm^{-3}: 10^{15} (a), 10^{16} (b), 10^{17} (c); $d_p = 150$ μm. Surface numbers are the same to Fig. 3.

Fig. 5. Ideality factor and its change as a function of the acceptor (boron) concentration and iron concentration. T, K: 290 (a), 340 (b); $d_p = 180$ μm. Surface numbers are the same to Fig. 3.

Fig. 6. (a) Typical dependencies of ideality factor on base thickness. The results for Fe$_i$B$_s$ and Fe$_i$ coexistence (curves 1–6, filled marks) as well as for unpaired Fe$_i$ sole (2a, 5a, 6a, empty marks) are presented. T, K: 290 (1, 2, 2a), 320 (3), 340 (4–6, 5a, 6a); N_{Fe}, cm^{-3}: 10^{10} (4, 5, 5a), 10^{12} (3), 10^{13} (1, 2, 2a, 6, 6a); N_A, cm^{-3}: 10^{15} (1, 3, 6, 6a), $3.162 \cdot 10^{15}$ (4), 10^{17} (2, 2a, 5, 5a). The marks are the simulation result, the lines are fitted curves using Eq. (6).

(b) Ideality factor thickness coefficient vs iron concentration. T, K: 290 (1, 2), 325 (3), 340 (4–6); N_A, cm^{-3}: 10^{15} (4), 10^{16} (1, 5), 10^{17} (2, 3, 6).

(c) Ideality factor thickness coefficient vs boron concentration. T, K: 290 (1, 2), 325 (2–5), 340 (6); N_{Fe}, cm^{-3}: 10^{10} (3, 6), 10^{11} (1, 4), 10^{12} (5), 10^{13} (2).

(d) Ideality factor thickness coefficient vs temperature. N_A, cm^{-3}: 10^{15} (1, 2), 10^{16} (3, 4), 10^{17} (5, 6). N_{Fe}, cm^{-3}: 10^{10} (3, 5), 10^{12} (2, 4, 6).

Panels (b)–(d) present results in the case of Fe$_i$B$_s$ and Fe$_i$ coexistence.

Fig. 7. The calculated dependencies of electron diffusion length in the structure base in case of unpaired Fe$_i$ sole. The shaded area represents values of base thickness, which used in simulation.

Fig. 8. The distribution of fraction of positively charged interstitial iron $N_{Fe_i^+}$ to the total impurity number N_{Fe} in structure base. The curves 1 and 2 correspond to the cases of lone unpaired Fe$_i$ and Fe$_i$B$_s$ and Fe$_i$ coexistence, respectively. The curve 3 is difference of 1 and 2. $T = 330$ K, $N_A = 3.162 \times 10^{15}$ cm^{-3}, $d_p = 180$ μm.

Table 1:

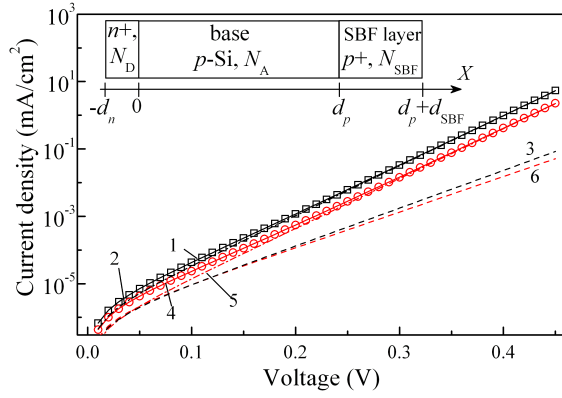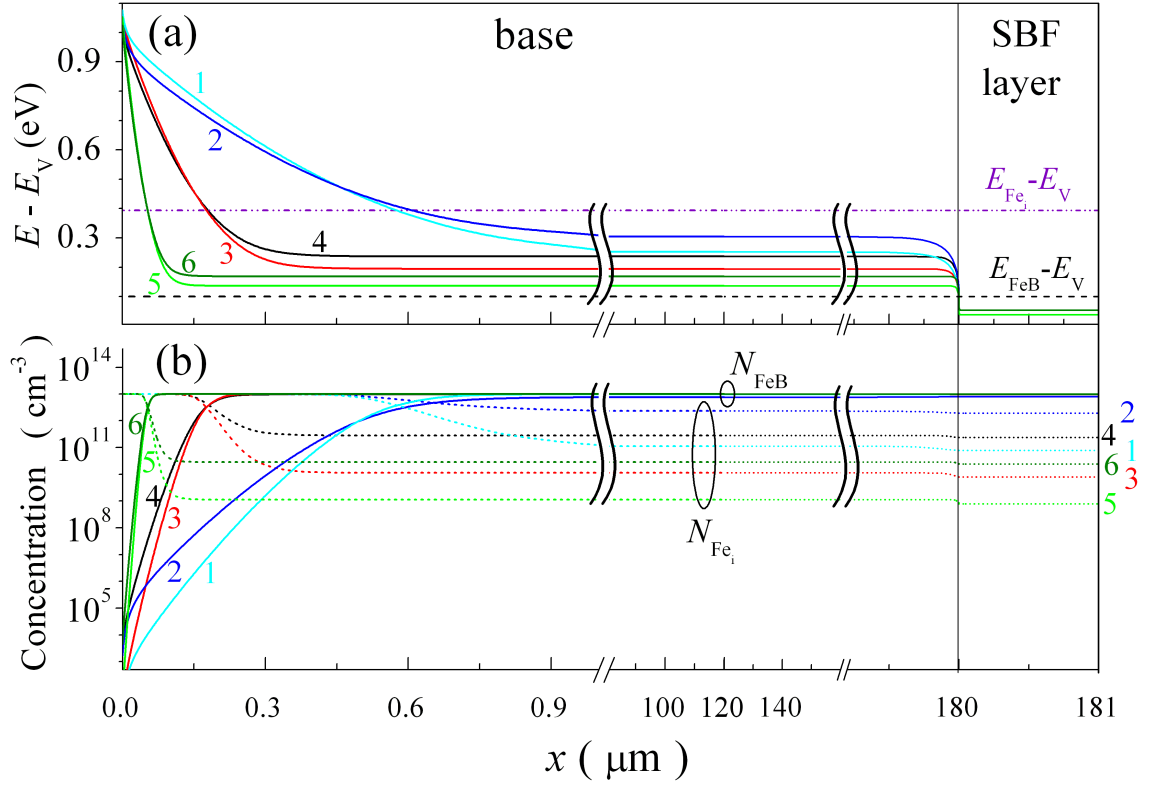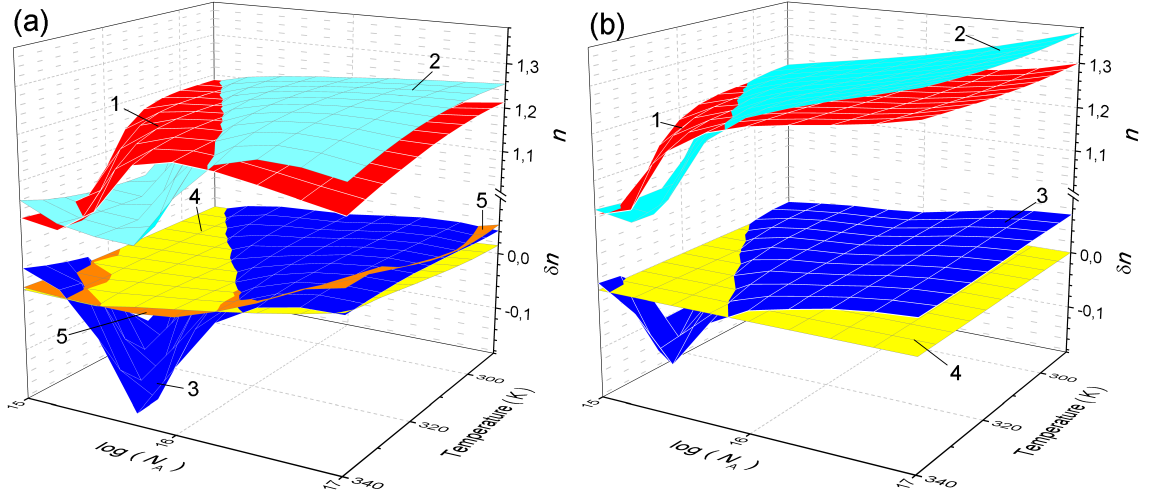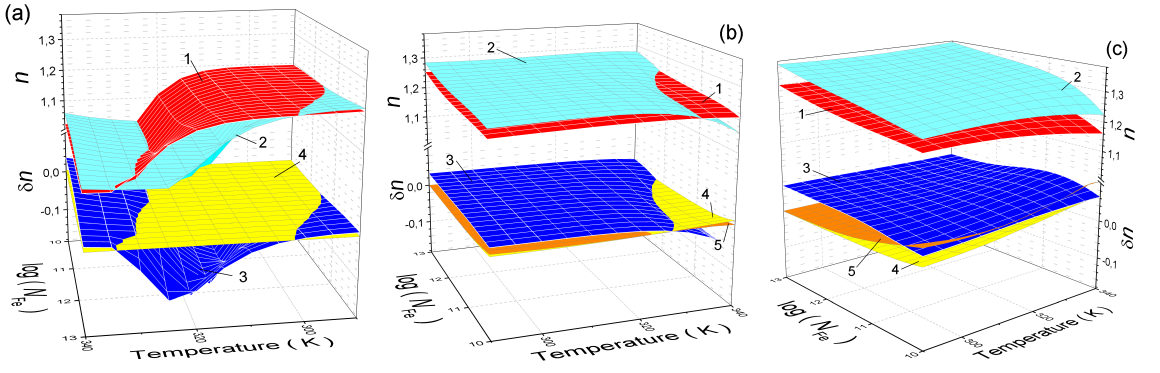| Parameter	Range	Number of values
d_n, μm	0.5	1
d_p, μm	$150 - 240$	4
d_{BSF}, μm	1	1
N_{D}, cm^{-3}	10^{19}	1
N_{A}, cm^{-3}	$10^{15} - 10^{17}$	9
N_{BSF}, cm^{-3}	$5 \cdot 10^{18}$	1
N_{Fe}, cm^{-3}	$10^{10} - 10^{13}$	19
T, K	$290 - 340$	11

Figure 1: .

Figure 2: .
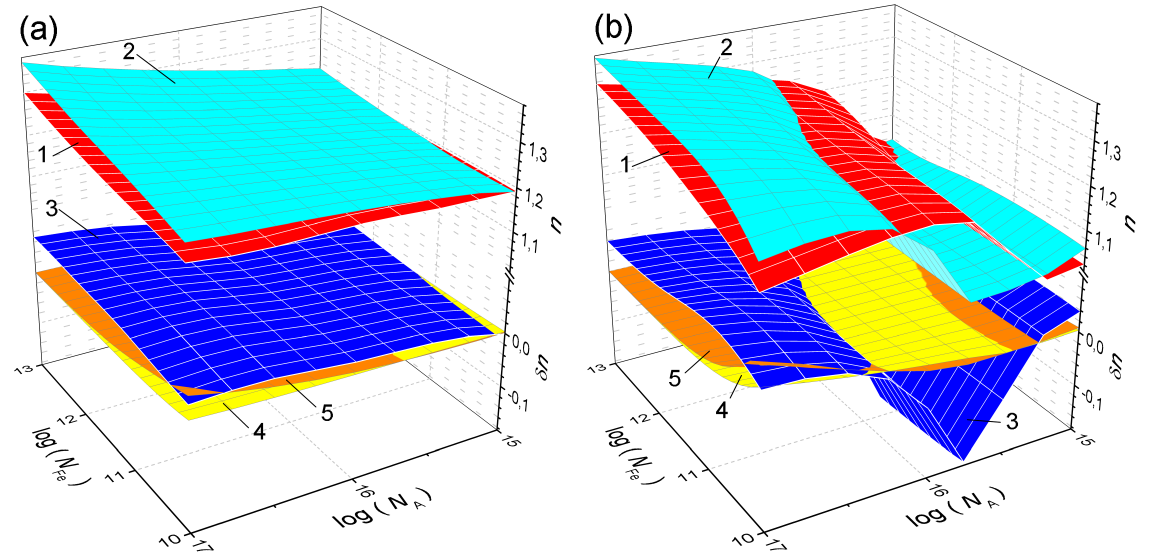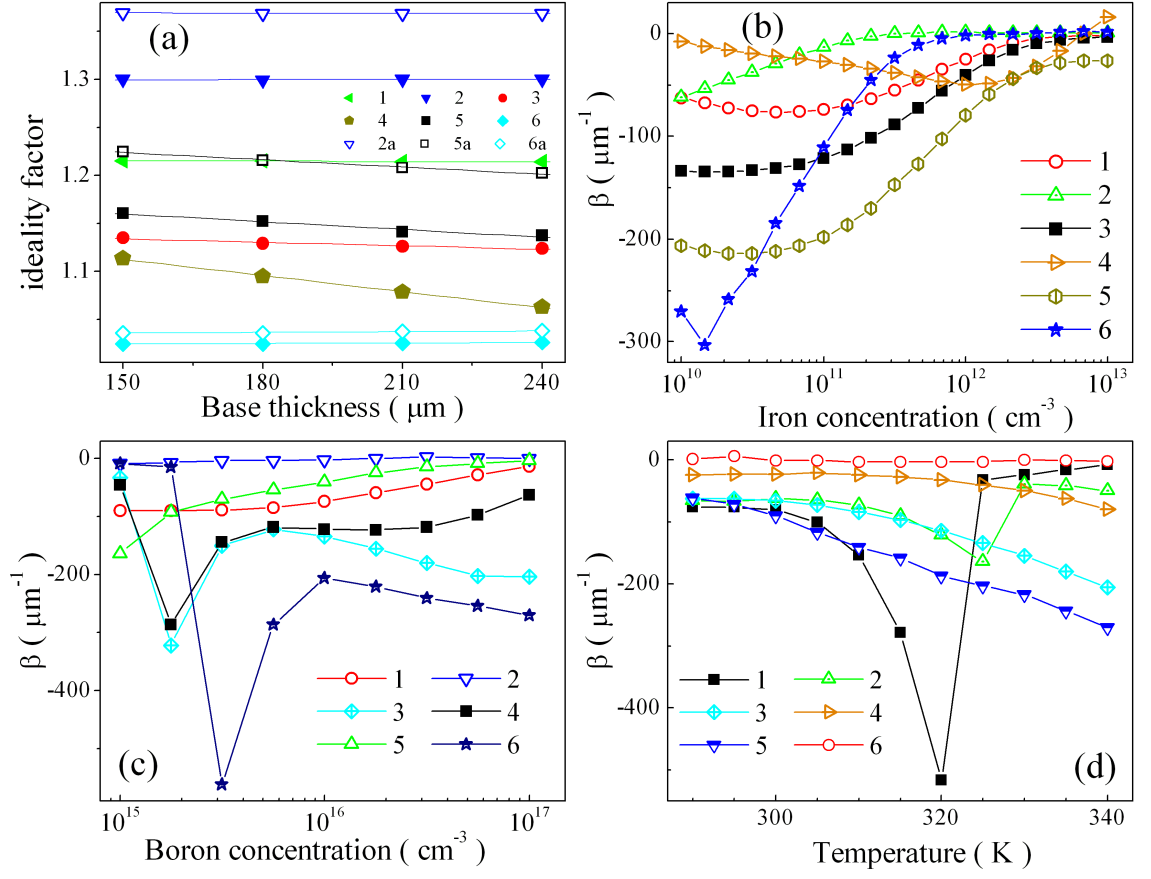
11

Figure 3: .

Figure 4: .
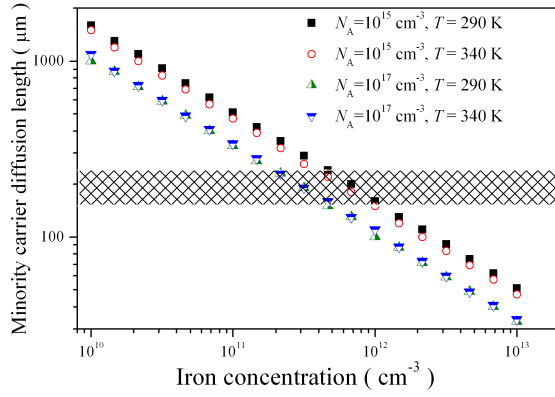

Figure 5: .

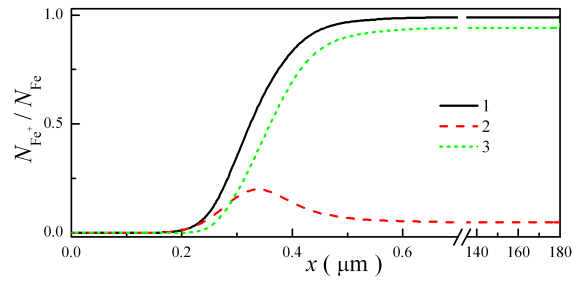Figure 6: .

Figure 7: .

Figure 8: .

Моделювання фактору неідеальності в n^+–p–p^+–Si структурах

О.Я. Оліх, О.В. Завгородній

Київський національний університет імені Тараса Шевченка
Україна, 01601, місто Київ, вул. Володимирська, 64/13
e-mail: olikh@univ.kiev.ua

У цій роботі подано результати моделювання величини фактору неідеальності кремнієвих $n^+ - p - p^+$ структур. При цьому вважалося, що основні рекомбінаційні центри у базі структури пов'язані з домішковими атомами заліза. Для моделювання вольт-амперних характеристик таких структур використовувався Solar Cells Capacitance Simulator (SCAPS). При цьому додатково враховувалися температурні залежності параметрів як матеріалу, так і дефектів. При розрахунках вар'ювалися величини рівня легування ($10^{15} \div 10^{17}$ см$^{-3}$ атомів бору) та товщини ($150 \div 240$ мкм) бази, температура ($290 \div 340$ К) та концентрації домішки заліза ($10^{10} \div 10^{13}$ см$^{-3}$). Окремо розглядалися випадки, коли всі атоми заліза знаходилися у міжвузольному положенні Fe$_i$ та коли переважна частина з них утворювала пари з легуючою домішкою Fe$_i$B$_s$. Останній випадок відповідає стану рівноваги за відсутності освітлення і при цьому співвідношення між концентраціями Fe$_i$ та Fe$_i$B$_s$ визначалося положенням рівня Фермі та температурою. Визначення величини фактору неідеальності (n) відбувалося шляхом апроксимації (з використанням метаеврістичного методу IJAVA) отриманих вольт–амперних характеристик.

Показано, що навіть за наявності Fe$_i$B$_s$ основну роль у формуванні величини n відіграють процеси рекомбінації за участю рівнів, пов'язаних з Fe$_i$. Залежності n від температури та рівня легування визначаються, насамперед, заселеністю рівня Fe$_i$. У випадку, коли підсилюється відносний внесок процесів власної рекомбінації (високі температури та рівень легування, низькі концентрації домішки) відбувається зменшення фактору неідеальності. На величину n, окрім концентрації дефектів, впливає також їх просторове розташування відносно $p - n$ переходу. Зі збільшенням товщини бази структури (у випадку, коли вона перевищує довжину дифузії неосновних носіїв та переважаючою є рекомбінація Шоклі-Ріда-Хола) відбувається незначне зменшення фактору неідеальності. Показано, що можуть реалізуватися випадки, коли n після розпаду Fe$_i$B$_s$ зменшується. Запропоновано, що зміна фактору неідеальності після розпаду Fe$_i$B$_s$, поряд з абсолютним значенням n, може бути використана для оцінки концентрації домішок.

Ключові слова: фактор неідеальності, кремній, n^+–p–p^+ структура, SCAPS, концентрація заліза